Implementation of the Williamson–Hall and Halder–Wagner Methods into RIETAN-FP

Fujio Izumi*, **, Takuji Ikeda***

*Guest Professor of Advanced Ceramics Research Center, Nagoya Institute of Technology
10-6-29, Asahigaoka, Tajimi, Gifu 507-0071, JAPAN
**National Institute for Materials Science
1-2-1 Sengen, Tsukuba, Ibaraki 305-0047, JAPAN
***National Institute of Advanced Industrial Science and Technology
4-2-1 Nigatake, Miyagino-ku, Sendai, Miyagi 983-8551, JAPAN

Abstract

Microstructural evaluation is important to understand physical and chemical properties of polycrystalline materials, particularly in the field of nanotechnology. The latest version of a multi-purpose pattern-fitting system, RIETAN-FP, offers new features of Williamson–Hall (WH) and Halder–Wagner (HW) methods to determine crystallite sizes and microstrains from integral breadths, β, evaluated after the Rietveld or Le Bail analysis of X-ray and neutron powder diffraction data. Contributions of instrumental broadening are subtracted with analytical results of instrumental standards showing negligible sample broadening. Gnuplot is used for the graphical representation of linear relationships: $\beta\cos\theta$ *vs*. $\sin\theta$ in the WH plot and $(\beta/\tan\theta)^2$ *vs*. $\beta/(\tan\theta\sin\theta)$ in the HW one. Deviations from the linear relationships can easily be recognized by the resulting graphs. With these two methods, the mean volume-weighted size, $\langle D\rangle_V$, of microcrystalline CeO_2 was determined at 29.96 nm (WH) and 28.92 nm (HW), which are in good agreement with values reported for the round-robin sample. The present new features concerning microstructural characterization must deliver added value to users of RIETAN-FP in both academic institutions and industries.

Key-words

Crystallite size, Microstrain, Powder diffraction, Williamson–Hall plot, Halder–Wagner plot, RIETAN-FP

1. Information extractable from powder diffraction data by whole-pattern fitting

The whole-pattern fitting of X-ray and neutron powder diffraction data is powerful means of characterization to obtain the following structural, microstructural, and compositional information:

(a) Lattice parameters,
(b) Crystal-structure parameters,
(c) Magnetic moment (neutron diffraction),
(d) Crystallite sizes [1],
(e) Microstrains [1],
(f) Mass fractions (multi-phase samples).
(g) Observed integrated intensities, $|F_o|^2$, for *ab initio* structure solution,
(h) Electron densities (X-ray diffraction),
(i) Densities of coherent-scattering lengths, b_c (neutron diffraction),

A multi-purpose pattern-fitting program, RIETAN-FP [2], is capable of evaluating all the above physical quantities. Quantities (a)–(f) result from Rietveld refinement [3] while quantities (a), (d), (e), and (g) are obtained by pattern decomposition, *i.e.,* Le Bail analysis [4] plus hybrid pattern decomposition in RIETAN-FP. Further, iterations of maximum-entropy method (MEM) analyses by Dysnomia [5] and while-pattern fitting by RIETAN-FP make it possible to determine distributions of electron and scattering-length densities, (h) and (i), in the unit cell [6].

Rietveld analysis can also be applied to the quantitative analysis of a mixture of crystalline materials (f); this feature is very important in the characterization of reaction products and quality control in industries. The content of amorphous materials can also be determined by addition of an internal standard material.

Thanks to the above wealth of functions, RIETAN-FP has been contributing to many studies in a variety of fields such as physics, chemistry, materials science, and earth science.

The present report deals with microstructural characterization, (d) and (e), with RIETAN-FP v2.6 or later, helping its users to understand details in procedures to determine crystallite sizes and microstrains after Rietveld or Le Bail analy-

sis. This new version provides us with powerful and convenient means of investigating microstructures from isotropic profile broadening by X-ray and neutron powder diffraction.

Crystallite-size broadening can be used to determine the crystallite size of less than 1 μm in materials. On the other hand, microstrains are caused by a distribution of both tensile and compressive forces, which causes broadening of diffraction profiles about the original position. Crystallite-size broadening follows a $1/\cos\theta$ function while strain-induced profile broadening has a $\tan\theta$ dependence [1], which allows us to separate these two effects in diffraction data over a wide 2θ range. In what follows, three different methods of microstructural analysis from powder diffraction data will be described.

2. Determination of crystallite sizes and microstrains from profile parameters

With RIETAN-FP, crystallite sizes and microstrains have been estimated in the same manner as GSAS [7] so far. That is, profile parameters in the pseudo-Voigt function of Thompson, Cox, and Hastings [8] are refined by the Rietveld or Le Bail method from powder diffraction data of an instrumental standard and an analysis sample to determine crystallite sizes and microstrains.

In the pseudo-Voigt function of Thompson *et al.* [8], the full-width at half maximum (FWHM), H_G, for the Gaussian component is represented by

$$H_G = [8\ln 2(U\tan^2\theta + V\tan\theta + W)]^{1/2}. \quad (1)$$

On the other hand, the FWHM of the Lorentzian one, H_L, is computed by

$$H_L = \frac{X}{\cos\theta} + Y\tan\theta, \quad (2)$$

where θ is the Bragg angle, and U, V, W, X, and Y are profile parameters to be refined by a method of nonlinear least squares. In both GSAS and RIETAN-FP, the unit of U, V, and W in Eq. (1) is $(\text{degrees})^2$ whereas that of X and Y in Eq. (2) is degrees.

Let K be the shape factor (dimensionless), λ the wavelength of the X-ray or neutron beam, r a constant ($=\pi/180=0.0174533$) to convert degrees into radians. Then, the crystallite size, D, is determined by

$$D = \frac{K\lambda}{rX} \quad (3)$$

with the unit of D being equal to that of λ. K depends on assumptions made during the derivations. Microstrains corresponding to the Gaussian and Lorentzian components are, respectively, computed by

$$\varepsilon_G = r[8\ln 2(U - U_i)]^{1/2}, \quad (4)$$

$$\varepsilon_L = r(Y - Y_i), \quad (5)$$

where U_i and Y_i are contributions of the instrument to U and Y, respectively. U_i and Y_i can be estimated by Rietveld analysis from diffraction data of a sample whose crystallinity is high enough to show negligible profile broadening due to the sample.

This simple method, however, suffers from possible errors due to strong correlations among profile parameters, U, V, W, X, and Y. In addition, no dependence of profile broadening on a function containing θ is graphically illustrated, which is unfavorable for finding variations in the data and anisotropic broadening of diffraction profiles.

To overcome such drawbacks of the methodology adopted in GSAS [7], the Williamson–Hall [9] and Halder–Wagner [10,11] methods have recently been added to the latest version of RIETAN-FP. With these two features, D and ε can easily be determined from integral breadths, β, defined as (peak area)/(peak intensity) after Rietveld or Le Bail analysis. Diffraction data measured with characteristic X-rays such as Cu $K\alpha$ radiation are good enough to get reliable D and ε values. Because the graphing of the two kinds of plots with free software, gnuplot [12], is supported in RIETAN-FP, additional information is obtainable on the characterization of powders by use of profile broadening, for example, anisotropic one depending on directions of scattering vectors.

3. Williamson–Hall method

Crystallites whose size, D, is less than *ca.* 1 μm exhibit profile broadening. The integral breadth (in radians), β_D, due to the effect of small crystallites is related to D *via* the so-called Scherrer equation [13],

$$\beta_D = \frac{K\lambda}{D\cos\theta}, \quad (6)$$

corresponding to Eq. (3).

The effect of isotropic microstrain, ε, on profile broadening can be derived by differentiating Bragg's law,

$$\lambda = 2d\sin\theta, \quad (7)$$

with respect to θ (in radians):

$$\Delta\theta = -\frac{\Delta d}{d}\tan\theta = -\varepsilon\tan\theta. \quad (8)$$

That is, profile broadening due to microstrain, $\varepsilon = \Delta d/d$ (d: lattice-plane spacing), is proportional to $\tan\theta$. Stokes and Wilson [14] pointed out that the integral breadth, β_ε, arising from isotropic microstrain is related to the integral breadth of the strain distribution, ξ, by

$$\beta_\varepsilon = 2\xi\tan\theta. \quad (9)$$

Comparison between Eq. (6) and Eq. (9) shows that the dependence of β_D on θ is quite different from that of β_ε.

Williamson and Hall [9] introduced a simple approximation that the integral breadth, β, due to both of small crystallite sizes and microstrains is simply the sum of Lorentzian component, β_D , and the Gaussian one, β_ε:

$$\beta = \beta_D + \beta_\varepsilon. \tag{10}$$

Thus, Eq. (6) and Eq. (9) are combined together to yield

$$\beta = C\varepsilon \tan\theta + \frac{K\lambda}{D\cos\theta}, \tag{11}$$

where C is the proportional constant to convert ξ into the microstrain ε. The value of C, which depends on the assumptions made concerning the nature of the inhomogeneous strain, lies between 4 and 5 [15], with C=4 corresponding to the maximum (upper limit) of strain [16,17]. In part of previous work, C was carelessly set at 2, which probably arose out of confusing ξ with ε. Multiplying both sides of Eq. (11) by cosθ, we obtain

$$\beta\cos\theta = C\varepsilon\sin\theta + \frac{K\lambda}{D}. \tag{12}$$

Equation (12) is regarded as a straight line, $y=ax+b$. A plot of $y = \beta\cos\theta$ against $x = \sin\theta$ is referred to as the Williamson–Hall (WH) plot since Williamson and Hall [9] proposed this methodology in 1953. However, this designation is somewhat unfair because Hall was the first to report the idea in 1949 [18]. The slope of the straight line is $C\varepsilon$ while its y intercept is $K\lambda/D$. Equation (12) holds true for isotropic line broadening.

If both of crystallite-size and microstrain profiles are Gaussian, then the plot is convex downward, having the same terminal slope at a high angle as the Lorentzian case and intercepting the y axis at $K\lambda/D$ [19].

The WH plot is a very useful diagnostic tool for learning the kind(s) of profile broadening and determining approximate values of D and ε.

Regrettably, various K values such as 0.89, 0.9, 0.94, and 1.0 have been arbitrarily used in the literature without any regard to the definition of the crystallite size. Ida *et al*. [20] derived the K value of 4/3 for the mean volume-weighted average size, $\langle D\rangle_V$, defined as the ratio of the mean forth power of D divided by the mean cube of D,

$$\langle D\rangle_V = \langle D^4\rangle/\langle D^3\rangle, \tag{13}$$

in the case of spherical crystallites. *Note that the K value of 4/3 is valid on the representation of profile broadening not by the FWHM but by the integral breadth, β,* in the same way as Eq. (12).

4. Halder–Wagner method

For the determination of D and ε, Halder and Wagner [10,11] proposed an alternative equation containing the integral breadth, β^*, of the reciprocal lattice point and the lattice-plane spacing, d^*, for the reciprocal cell:

$$\left(\frac{\beta^*}{d^*}\right)^2 = \frac{K}{D}\cdot\frac{\beta^*}{(d^*)^2} + (2\varepsilon)^2 \tag{14}$$

with

$$\beta^* = \frac{\beta\cos\theta}{\lambda}, \tag{15}$$

$$d^* = \frac{2\sin\theta}{\lambda} \tag{16}$$

on the assumptions that the Lorentzian and Gaussian components of β^* are solely due to the size and strain effects, respectively. Equation (14) can be rewritten as

$$\left(\frac{\beta}{\tan\theta}\right)^2 = \frac{K\lambda}{D}\cdot\frac{\beta}{\tan\theta\sin\theta} + 16\varepsilon^2 \tag{17}$$

on the basis of direct space. Inside RIETAN-FP, another equation

$$\left(\frac{\beta\cos\theta}{\sin\theta}\right)^2 = \frac{K\lambda}{D}\cdot\frac{\beta\cos\theta}{\sin^2\theta} + 16\varepsilon^2 \tag{18}$$

equivalent to Eq. (17) is used because both of Eq. (12) and Eq. (18) contain sinθ and βcosθ. Equation (17) has a form of a straight line, $y=ax+b$, in a similar manner as Eq. (12). In the Halder–Wagner (HW) plot, $y = (\beta/\tan\theta)^2$ is plotted against $x = \beta/(\tan\theta\sin\theta)$. Then, the slope and y intercept of the resulting straight line afford $K\lambda/D$ and $16\varepsilon^2$, respectively. As described in the previous section, the value of K = 4/3 [20] is believed to be valid on the definition of the crystallite size as the volume-weighted average one for spherical crystallites.

Despite the approximations and assumptions made on the derivation of Eq. (17), the HW plot has a great advantage that data for reflections at low and intermediates angles are given more weight than those at higher diffraction angles, which are often less reliable. Further, Eq. (17) does not contain the constant C unlike Eq. (12), which is another advantage of the HW plot over the WH one.

5. Procedures of calculating crystallite sizes and microstrains in RIETAN-FP

In what follows, 'hoge' is the metasyntactic variable that should be replaced by a string (usually a sample name); hoge.ins is a user input file, hoge.int is an intensity data file, hoge.lst is a standard-output file, hoge.gpd is a gnuplot data file, and hoge.plot is a gnuplot script file consisting of commands of gnuplot.

5.1 An instrumental standard

After Rietveld or Le Bail analysis with a pair of files, hoge.ins and hoge.int, has been finished, sinθ and β(instr) cosθ, where β(instr) denotes the integral breadth due to the instrument, are estimated for all the reflections observed in the whole diffraction pattern and output to the gnuplot data file, hoge.gpd. Profile broadening arising from the instrument

includes spectral distribution of X-ray and neutron beams, deviations from the ideal geometry, axial divergence, sample transparency, *etc*. In all profile functions, $G(\Delta 2\theta)$ used in RIETAN-FP, the peak area of each reflection is normalized in such a way that

$$\int_{-\infty}^{+\infty} G(\Delta 2\theta)\,\mathrm{d}(2\theta) = 1. \qquad (19)$$

Therefore, β is simply equal to the reciprocal of the peak intensity.

Equations (12) and (17) are calculated from $\sin\theta$ and β(instr)$\cos\theta$, which is followed by linear regression analysis to obtain D and ε from the slope and y intercept. The D and ε values, which are output to hoge.lst, are expected to give an approximately straight line, which can easily be checked by drawing a graph by gnuplot with a pair of files, hoge.gpd and hoge.plt, created by RIETAN-FP. Commands in hoge.plt may be freely modified by the user to change the appearance of the graph.

An instrumental standard having the same crystal structure and chemical composition is preferred, of course. Unless such a sample of high crystallinity is available, a standard reference material such as NIST SRM 640 (Si) and SRM 660 (LaB_6) with a similar linear attenuation coefficient, μ, may be used as a substitute. Such a caution is demanded particularly when a sample of a small μ value is mounted on a flat-plate holder in an X-ray powder diffractometer with the Bragg–Brentano geometry where the effect of sample transparency is appreciable.

5.2 A sample showing broadened diffraction profiles

The hoge.gpd file for the instrument standard sample is renamed instrument.gpd and copied into a folder where a series of files, *e.g.*, hoge.ins and hoge.int, for an analysis sample are contained. If needed, one or more lines storing *hkl*, $\sin\theta$, $\beta\cos\theta$, *etc*. for another instrument standard may be inserted into instrument.gpd to complement reflection data in a low-angle region. Then, Rietveld or Le Bail analysis is carried out to obtain $\sin\theta$ and β(obs)$\cos\theta$. The $\sin\theta$ and β(instr)$\cos\theta$ values are input from instrument.gpd and interpolated by spline interpolation to give β(instr)$\cos\theta$ corresponding to the present sample. Such a procedure is very convenient, requiring only instrument.gpd.

Strictly speaking, the observed profile is the convolution of profiles due to the instrument and the sample. To evaluate the approximate contribution of the broadening, β(sample), originating in the sample, the following approximation formula is used:

$$[\beta(\text{sample})]^n = [\beta(\text{obs})]^n - [\beta(\text{instr})]^n. \qquad (20)$$

The power, n, is input by the user in hoge.ins. In happy and special situations, n is 1 for Lorentzian instrumental and sample broadening and 2 for Gaussian instrumental and sample broadening [19]. In the case of the intermediate character (Voigtian instrumental and sample broadening), n is expected to lie between 1 and 2. Equations (12) and (17) are then calculated from a set of $\sin\theta$ and β(sample)$\cos\theta$ pairs, which is followed by linear regression analysis to yield D and ε. Of course, graphing of the plot with gnuplot is also possible in this case because both $\sin\theta$ and β(sample)$\cos\theta$ for all the reflections in the whole 2θ range are output to hoge.gpd together with the corresponding script file, hoge.plt, for gnuplot. Deviations from the linear relationships, *i.e.*, Eq. (12) and Eq. (17), because of anisotropic profile broadening can easily be recognized by the resulting graph.

6. Determination of a crystallite size with diffraction data of CeO_2

The features of the WH and HW methods in RIETAN-FP v2.6 were tested with two sets of X-ray powder diffraction data for CeO_2: a broadened sample and an instrumental standard used for the first size/strain round robin [17]. These two intensity data (a "common" instrumental setup with Cu $K\alpha$ radiation) were downloaded from a Web page of the round robin [21].

Nanocrystalline CeO_2 exhibiting profile broadening due to the crystallite-size effect was produced by the thermal treatment of hydrated ceria at 923 K for 45 h [22]. Substantial strain is expected to be absent in this sample. The instrumental standard was prepared by annealing commercially available CeO_2 at 1573 K for 3 h in air.

With RIETAN-FP v2.6, the two intensity data were analyzed by the Rietveld method to determine the crystallite size and microstrain of the annealed sample of CeO_2 according to the procedures described in Sect. 5. The n value in Eq. (20) was set at 2.

Figure 1 illustrates the HW plot drawn from the two sets of the Rietveld refinement. A distinct linear relationship is found between $(\beta/\tan\theta)^2$ and $\beta/(\tan\theta\sin\theta)$. The y intercept is as small as 9.443×10^{-6}, corresponding to a very small microstrain of 0.07682 % in this sample annealed at the high temperature. The WH plot also showed that $\beta\cos\theta$ bears a linear relationship to $\sin\theta$. The upper limit of ε was estimated at 0.4957 % from the slope of the resultant straight line with $C = 4$. This strain value is comparable to the average one, 0.4(9) %, in the round robin [21].

The crystallite sizes determined by the WH and HW methods were $22.47K$ nm and $21.69K$ nm, respectively. K depends on the definition of the crystallite size. If the K

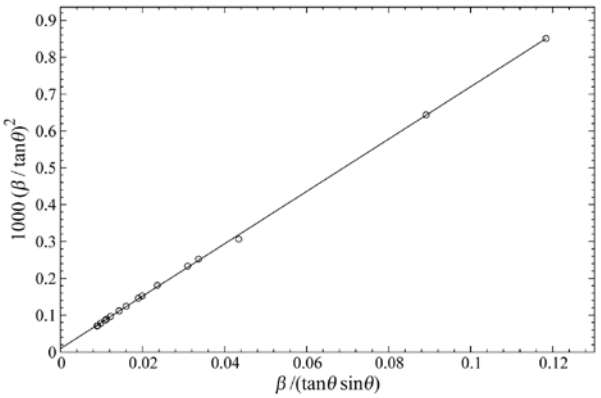

Fig. 1 The Halder–Wagner plot for the round-robin sample of nanocrystalline CeO_2. The straight line was obtained by linear regression analysis. Note that $(\beta/\tan\theta)^2$ is multiplied by 1000.

value of 4/3 for the mean volume-weighted size of spherical crystallites [20] is adopted, $\langle D\rangle_V$ is calculated at 29.96 nm in the WH method and 28.92 nm in the HW one. These two values slightly less than 30 nm fall within ranges of $\langle D\rangle_V$, (32±11) nm, reported by Balzar *et al.* [17] and are comparable to $\langle D\rangle_V$ determined by a fundamental-parameter approach [23] (see Fig. 4 in Ref. 17).

7. Conclusion

The WH and HW plots, which have recently been implemented into RIETAN-FP v2.6 or later, are the most rapid diagnostic tools for determining the kind(s) of profile broadening present in samples analyzed by the Rietveld or Le Bail method [19]. Both of them present the following valuable information about microstructures of various polycrystalline materials:

(a) Clear discrimination between crystallite-size and microstrain effects,
(b) An estimate of the crystallite size, D,
(c) An estimate of the microstrain, ε,
(d) Clear distinction between isotropic (monotonic curve) and anisotropic (scatter) broadening by graphical representation with gnuplot.

For example, (b) and (c) are useful to characterize nanocrystalline materials showing marked surface effects while (c) helps us to estimate the degree of inhomogeneous distribution of solute atoms in solid solutions. With only numerical data, anisotropic broadening cannot be well perceived contrary to (d). We are confident that the present new features of microstructural characterization in RIETAN-FP deliver added value to its users in both academic institutions and industries.

Acknowledgments

We thank professor Takashi Ida of Nagoya Institute of Technology for fruitful discussion on the analysis of crystallite sizes and microstrains and Dr. Manabu Inukai of Nagoya Institute of Technology for letting us know of the HW method.

References

[1] R. Jenkins, R. L. Snyder, "Introduction to X-ray Powder Diffractometry," John Wiley & Sons, Inc., New York (1996) pp. 89–91.
[2] F. Izumi, K. Momma, Solid State Phenom. 130 (2007) 15–20.
[3] "The Rietveld Method," ed. by R. A. Young, Oxford University Press (1995).
[4] A. Le Bail, H. Duroi, J. L. Fourquet, Mater. Res. Bull. 23 (1988) 447–452.
[5] K. Momma, T. Ikeda, A.A. Belik, F. Izumi, Powder Diffr. 28 (2013) 184–193.
[6] F. Izumi, Solid State Ionics 172 (2004) 1–6.
[7] A. C. Larson, R. B. Von Dreele, "General Structure Analysis System (GSAS)," Report LAUR 86-748, Los Alamos National Laboratory, Los Alamos (2004) pp. 162–164.
[8] P. Thompson, D. E. Cox, J. B. Hastings, J. Appl. Crystallogr. 20 (1987) 79–83.
[9] G. K. Williamson, W. H. Hall, Acta Metall. 1 (1953) 22–31.
[10] N. C. Halder, C. N. J. Wagner, Acta Crystallogr. 20 (1966) 312–313.
[11] N. C. Halder, C. N. J. Wagner, Adv. X-Ray Anal. 9 (1966) 91–102.
[12] http://gnuplot.sourceforge.net/
[13] P. Scherrer, Nachr. Ges. Wiss. Göttingen, Math.-Phys. Klasse 2 (1918) 96–100.
[14] A. R. Stokes, A. J. C. Wilson, Proc. Cambridge Philos. Soc. 40 (1944) 197–198.
[15] http://pd.chem.ucl.ac.uk/pdnn/peaks/size.htm
[16] A. R. Stokes, A. J. C. Wilson, Proc. Phys. Soc. (London, U. K.) 56 (1944) 174–181.
[17] D. Balzar, N. Audebrand, M. R. Daymond, A. Fitch, A. Hewat, J. I. Langford, A. Le Bail, D. Louër, O. Masson, C. N. McCowan, N. C. Popa, P. W. Stephens, B. H. Toby, J. Appl. Crystallogr. 37 (2004) 911–924.
[18] W. H. Hall, Proc. Phys. Soc. A (London, U. K.) 62 (1949) 741–743.
[19] E. H. Kisi, C. J. Howard, "Applications of Neutron Powder Diffraction," Oxford University Press, New York

(2008) Chap. 9.
[20] T. Ida, S. Shimazaki, H. Hibino, H. Toraya, J. Appl. Crystallogr. 36 (2003) 1107–1115.
[21] http://www.ccp14.ac.uk/ccp/web-mirrors/balzar/div853/balzar/s-s_rr.htm
[22] N. Audebrand, J.-P. Auffrédic, D. Louër, Chem. Mater. 12 (2000) 1791–1799.
[23] R. W. Cheary, A. Coelho, J. Appl. Crystallogr. 25 (1992) 109–121.